Available online at www.sciencedirect.com
SCIENCE DIRECT®
Journal of Organometallic Chemistry 673 (2003) 47–55
Journal of Organometallic Chemistry
www.elsevier.com/locate/jorganchem

Group 10 metal compounds of 1,1′-bis(diphenylphosphino)ferrocene (dppf) and 1,1′-bis(diphenylphosphino)ruthenocene: a structural and electrochemical investigation. X-ray structures of $[MCl_2(dppr)]$ (M = Ni, Pd)☆

Chip Nataro [a,*], Alison N. Campbell [a], Michelle A. Ferguson [a], Christopher D. Incarvito [b,1], Arnold L. Rheingold [b,2]

[a] Department of Chemistry, Lafayette College, Easton, PA 18042, USA
[b] Department of Chemistry and Biochemistry, University of Delaware, Newark, DE 19716, USA

Received 30 December 2002; received in revised form 10 March 2003; accepted 11 March 2003

Abstract

The oxidative electrochemistry of 1,1′-bis(diphenylphosphino)ferrocene (dppf) and 1,1′-bis(diphenylphosphino)ruthenocene (dppr) was investigated at a variety of temperatures and concentrations. In addition, the oxidative electrochemistry of $[NiCl_2(dppf)]$ and $[MCl_2(dppr)]$ (M = Ni, Pd or Pt) compounds was studied. During the preparation of the dppr compounds, crystals of $[NiCl_2(dppr)]$ and $[(PdCl_2(dppr)]\cdot CH_2Cl_2$ were obtained and the structures were determined. With the previously determined structures of $[MCl_2(dppf)]$ (M = Ni, Pd or Pt) and $[PtCl_2(dppr)]$, a thorough examination of the binding of dppf and dppr to Group 10 metals was performed.

Keywords: Electrochemistry; 1,1′-bis(diphenylphosphino)ferrocene; 1,1′-bis(diphenylphosphino)ruthenocene; Crystal structures; Cyclic voltammetry; Supporting electrolyte

1. Introduction

The bidentate phosphine 1,1'-bis(diphenylphosphino)ferrocene (dppf) has been extensively studied, particularly as a ligand in transition metal catalysts [1]. The redox active ferrocene backbone of dppf provides an area of specific interest, because it has been proposed to influence the electron transfer properties of dppf containing compounds [2]. However, unlike ferrocene, the oxidation of dppf is not completely reversible. The oxidative electrochemistry of dppf has been studied in acetonitrile (MeCN) [3–5], dichloromethane (DCM) [6] and 1,2-dichloroethane (DCE) [7–9]. DuBois et al. have demonstrated that, at a glassy carbon electrode, an irreversible chemical reaction occurs after the oxidation of dppf in MeCN [3]. Contrary to DuBois, Housecroft et al. observed reversible oxidative electrochemistry of dppf at scan rates from 0.02 to 0.2 V s^{-1} with peak separations similar to ferrocene using a Pt bead electrode [4]. In a related study, the oxidative electrochemistry of dppf in a solution of 5% DCM in MeCN displayed an oxidation which was followed by an irreversible chemical reaction at scan rates less than 5 V s^{-1} [5]. Three studies performed using DCM as the solvent have all concluded the oxidation of dppf is chemically irreversible [6].

The oxidative electrochemistry of dppf has been most thoroughly studied in DCE. The initial report states that dppf 'undergoes an essentially reversible one-electron

☆ Presented in part at the 224th National Meeting of the American Chemical Society, Boston, MA, August 18–22, 2002, see: Abstracts of Papers, INOR 375 and INORG 380.

* Corresponding author. Tel.: +610-330-5216; fax: +610-330-5714.
E-mail address: nataroc@lafayette.edu (C. Nataro).
[1] Current address: Department of Chemistry, Yale University, New Haven, CT, USA.
[2] Current address: Department of Chemistry and Biochemistry, University of San Diego, La Jolla, CA, USA.

0022-328X/03/$ - see front matter © 2003 Elsevier Science B.V. All rights reserved.
doi:10.1016/S0022-328X(03)00155-4

oxidation followed by a fast chemical reaction' [7]. This study was followed by a report in which the oxidized form of dppf was determined to undergo a dimerization [8]. A variety of temperatures and concentrations were investigated and activation parameters for this dimerization were reported. One complication in the dimerization study by Pilloni is that the electrochemically-generated $dppf^+$ undergoes reactions other than dimerization [8]. The $dppf^+$ can react with adventitious water or more significantly, the perchlorate supporting electrolyte. The authors admit the transfer of an oxygen atom from the perchlorate is involved in the decay of the ferrocenyl cation [8]. Therefore, the rate constants and activation parameters determined in that study should be sensitive to the presence of the perchlorate anion. A more recent study of the oxidation of dppf in DCE, did not report any information regarding the reversibility was reported [9].

As the electrochemical behavior of dppf has been studied so extensively, it is somewhat surprising that the electrochemistry of the ruthenium analogue, 1,1′-bis(diphenylphosphino)ruthenocene (dppr), has not been investigated. This may be due to the apparent irreversibility of the parent ruthenium compound, ruthenocene. The oxidation of ruthenocene was thought to be irreversible until Mann reported that the oxidation is reversible when large, weakly-coordinating ions are used as the anion of the supporting electrolyte [10].

There are also no known reports of the electrochemistry of dppr-containing compounds. Studies that used dppr-containing compounds have focused on catalytic applications, typically in comparison to dppf analogues. For example, the coupling of PhMgBr with 1,2-dibromobenzene is faster and gives higher yields when using [$PdCl_2$(dppr)], as compared to [$PdCl_2$(dppf)] as the catalyst [11]. An opposing trend is seen in the coupling of H_2NBu with p-BuC_6H_4Br, where dppf is a more efficient ligand than dppr [12]. In these and other examples, the difference in reactivity has been attributed to the larger bite angle of dppr, as compared to dppf [13].

To probe the electronic behavior of dppf and dppr, the oxidative electrochemistry of dppf, dppr, [$NiCl_2$(dppf)] and [MCl_2(dppr)] (M = Ni, Pd and Pt) was investigated using cyclic voltammetry. The electrochemistry of [MCl_2(dppf)] (M = Pd and Pt) has been reported [7], and the structures of [MCl_2(dppf)] (M = Ni [14], Pd [15] and Pt [16]) and [$PtCl_2$(dppr)] [11] have been previously determined. The geometry around the metal centers differs; the Ni is tetrahedral and the Pd and Pt are square planar. In preparing the compounds for the electrochemical studies, crystals of [MCl_2(dppr)] (M = Ni and Pd) were obtained and the structures determined. Examining this series of structures provides the opportunity to investigate the effects of bonding dppr and dppf to the Group 10 metals. By examining the electronic and steric factors, we hope to gain a better understanding of the differences in catalytic activity of dppr and dppf.

2. Results and discussion

The oxidative electrochemistry of dppf at a variety of temperatures and concentrations shows a single, chemically irreversible wave (Fig. 1). The electrochemical parameter, E_L(L) is defined as $1/2E^0(Fe^{III}/Fe^{II})$ (vs. NHE) for symmetric ferrocenes and estimates how substitution of the Cp rings of ferrocene effects the $E_{1/2}$ [17]. For dppf, E_L(L) has been determined to be 0.45 V. The E_L(L) for ferrocene systems can also be estimated using the equation $E_L(\text{calc.}) = 0.45\sigma_p + 0.36$ where σ_p is the Hammett substituent constant for the functional group on ferrocene [17]. The σ_p for the $-PPh_2$ group is 0.19 [18] giving an E_L(calc.) of 0.45 V, which is in excellent agreement with the experimental value.

The chemical reversibility of the oxidation of dppf is dependent on the temperature, scan rate and, most importantly, analyte concentration. At scan rates less than 300 mV s^{-1}, the oxidation product undergoes a dimerization reaction, which is proposed to produce $[dppf_2]^{2+}$ [8]. The exact structure of this dimer is currently under investigation in these labs. The chemical reversibility parameter (i_r/i_f) for the electrochemical dimerization [19] was calculated for all temperatures and concentrations in this study. The values obtained at a scan rate of 50 mV s^{-1} are shown in Table 1. The values of i_r/i_f indicate that the oxidation is more reversible under the conditions used in this study than in the previous study in DCE [8]. In that study, tetrabutylammonium perchlorate was used as the supporting electrolyte even though the perchlorate anion reacts with the dppf oxidation product. The differences in the i_r/i_f values are likely due to the differences in the dielectric constants for DCM (8.93) and DCE (10.42) [20] and/or the non-interacting supporting electrolyte [21].

The values of i_r/i_f were used to determine the second order rate constant (k_D) for the dimerization [22]. Average values of k_D were determined for each temperature and are listed in Table 1, along with the average deviations from the mean. The experimental data was simulated using DigiSim, and a good fit was obtained using a dimerization mechanism (Fig. 2). Simulated values for k_D compared favorably to the experimental values. The experimental and simulated values of k_D can be related to activation parameters through an Arrhenius relationship (Fig. 3). The values obtained for $\Delta H^{\ddagger}$ and $\Delta S^{\ddagger}$ were 25(1) kJ mol^{-1} and $-220(10)$ J (mol K)$^{-1}$ for the experimental data and 26(1) kJ mol^{-1} and -220 J (mol K)$^{-1}$ for the simulated. The previously reported activation parameters in DCE with the per-

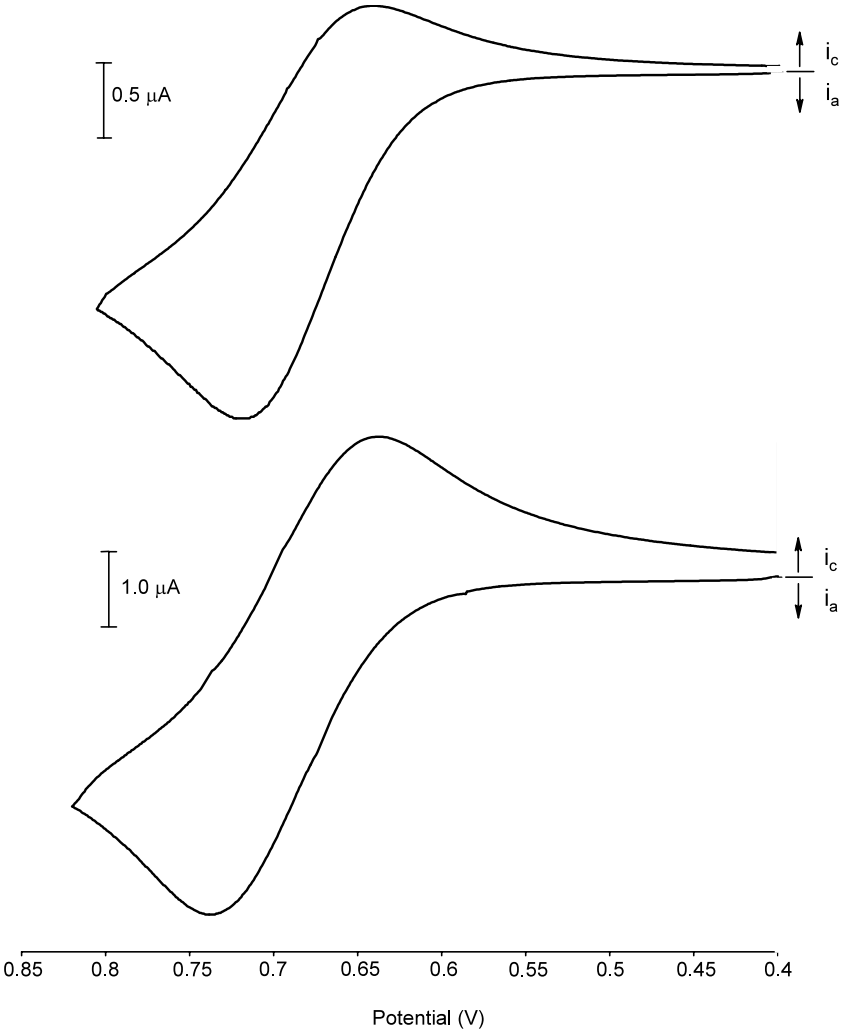

Fig. 1. CV scans of the oxidation of 1.0 mM dppf in DCM/0.05 M $[NBu_4]^+[B(C_6F_5)_4]^-$ at 273 K at two different scan rates: (top) 25 mV s^{-1}; (bottom) 100 mV s^{-1}.

Table 1
Reversibility and second order rate constants for the oxidation of dppf

	−10 °C	0 °C	10 °C	20 °C
Reversibility (i_r/i_f)				
0.50 (mM)	91	88	83	76
1.0 (mM)	83	79	71	64
5.0 (mM)	74	68	66	61
10 (mM)	73	59	56	54
Rate constant [10^2 k_D (M^{-1} s^{-1})]				
Experimental	1.5(0.3)	2.2(0.5)	3.5(0.5)	5.3(0.5)
Simulated	1.2(0.2)	1.8(0.1)	2.7(0.3)	4.5(0.5)

chlorate supporting electrolyte were 19 kJ mol^{-1} for $\Delta H^{\ddagger}$ and −130 J (mol K)$^{-1}$ for $\Delta S^{\ddagger}$ [8]. Comparing these values indicates the dimerization is less favorable in DCM with $[NBu_4]^+[B(C_6F_5)^-]$ supporting electrolyte.

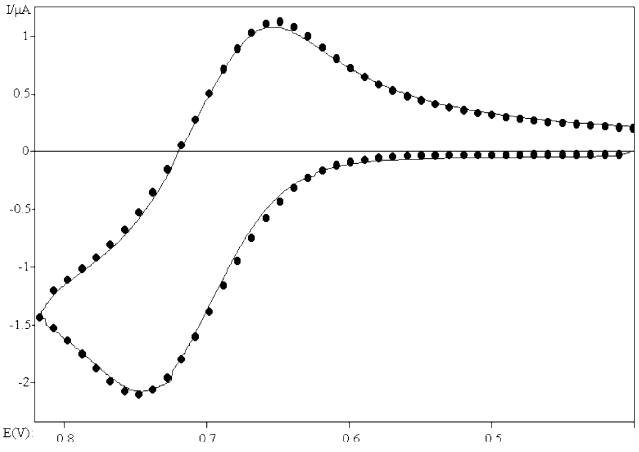

Fig. 2. Comparison of experimental (–) and simulated (●) cyclic voltammogram for oxidation of dppf in DCM at 263 K with concentration 0.50 mM and $v = 100$ mV s^{-1}. Simulation parameters were $E_{1/2} = 0.685$ V, $k_s = 0.1$ cm s^{-1}, $1-\alpha = 0.35$, dimerization $K_{eq} = 1 \times 10^5$, $k_{D(17)} = 180$ (M^{-1} s^{-1}), $R_u = 9000$, $C_{dl} = 0.03$ μF.

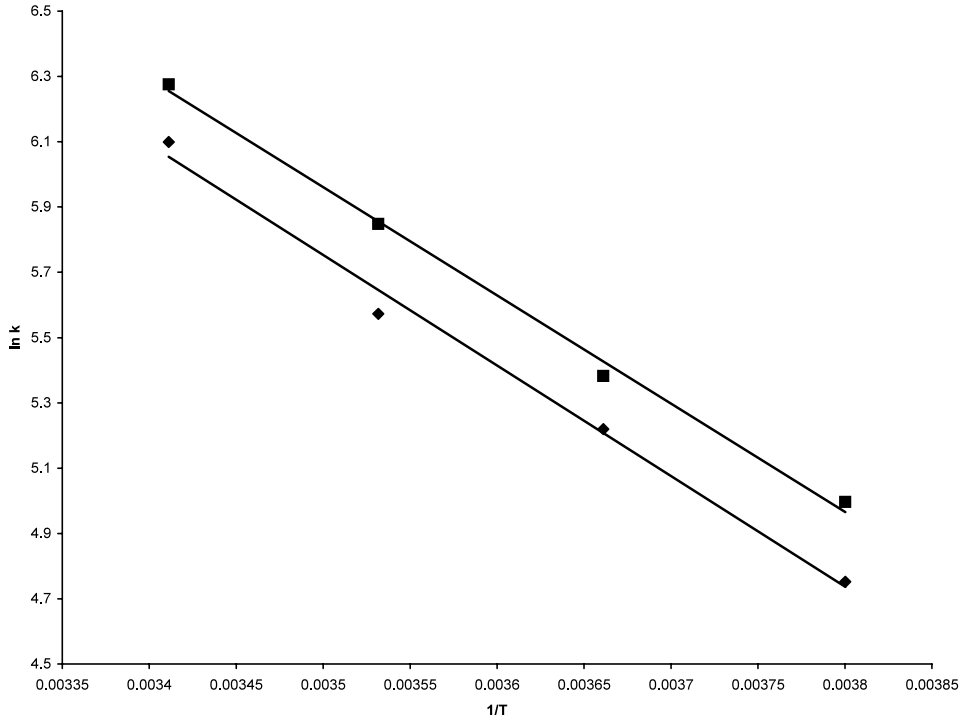

Fig. 3. Arrhenius plot of experimental (■) and simulated (◆) data. For the experimental data slope = -3.32×10^3, intercept = 17.6 and $R^2 = 0.996$ and for the simulated data the slope = -3.39×10^3, intercept = 17.6 and $R^2 = 0.992$.

The oxidative electrochemistry of dppf is different from that of ferrocene, and a similar pattern is observed for the ruthenium analogues. Both ruthenocene and dppr have more positive oxidation potentials than the corresponding iron compounds, however the potential difference between ruthenocene and ferrocene is substantially larger, 0.41 V [23]. Unlike the iron system, the oxidation potentials of dppr and ruthenocene are essentially identical, differing by only 0.03 V. The oxidation of ruthenocene is reversible only when supporting electrolytes with large anions such as $[NBu_4][B(C_6H_3(CF_3)_2)_4]$ [10] and $[NBu_4][B(C_6F_5)_4]$ [23] are used. The irreversibility of ruthenocene in the presence of smaller anions is attributed to the enhanced reactivity of Cp_2Ru^+ due to the larger separation between the Cp rings, as compared to ferrocene [10]. This enhanced reactivity can be sterically inhibited as in decamethylruthenocene, which exhibits a reversible oxidation under a variety of conditions [24]. Two $-PPh_2$ groups are clearly not bulky enough to prevent follow-up reactions, as the oxidation of dppr is irreversible when $[NBu_4][B(C_6F_5)_4]$ is used as the supporting electrolyte (Fig. 4). In addition, the $-PPh_2$ group may provide additional reaction pathways as seen in the oxidation of dppf [8].

The series of dppr containing Group 10 metal compounds, $[M(Cl_2(dppr)]$ (M = Ni, Pd and Pt), have been prepared and characterized [11]. As with the dppf analogue [7], $[NiCl_2(dppr)]$ was previously determined to be paramagnetic, however the magnetic moment was not determined [11]. The Evans method [25] was used to determine the magnetic moment, which is 2.8 μ_B [26]. While slightly smaller than the value of 3.7 μ_B obtained for the dppf analogue [7], this is still within the expected range for Ni(II) compounds [27]. As additional means of characterization, the UV–Vis spectrum was obtained.

The λ_{max} for $[NiCl_2(dppf)]$ has been attributed to the ferrocene unit [7], and the λ_{max} for $[NiCl_2(dppr)]$ occurs at the same wavelength. This is somewhat surprising as the λ_{max} for ruthenocene occurs at a substantially lower wavelength than that of ferrocene [28]. However, the λ_{max} values of $Pt(PPh_3)_2(Fe(C_5H_4S)_2)$ and $Pt(PPh_3)_2(Ru(C_5H_4S)_2)$ are nearly identical and are attributed to the metallocenes [29]. The two remaining bands in the spectrum of $[NiCl_2(dppf)]$ are attributed to a dichlorobisphosphino d^8 metal [7] and similar bands are observed in the spectrum of $[NiCl_2(dppr)]$.

During the preparation of $[NiCl_2(dppr)]$ and $[PdCl_2(dppr)]$, crystals suitable for X-ray analysis were obtained. A distorted tetrahedral geometry was found for the Ni in $[NiCl_2(dppr)]$ as anticipated for a d^8 paramagnetic compound (Fig. 5). The geometry around the Pd in diamagnetic $[PdCl_2(dppr)]$ was determined to be square planar (Fig. 6). Selected structural parameters for these two compounds as well as $[PtCl_2(dppr)]$ and $[MCl_2(dppf)]$ (M = Ni, Pd and Pt) are presented in Table 2. Some of the measurements for $[NiCl_2(dppf)]$ and $[PtCl_2(dppr)]$ were not listed in the original reports and were determined using ORTEP-3 for Windows version 1.076 [30].

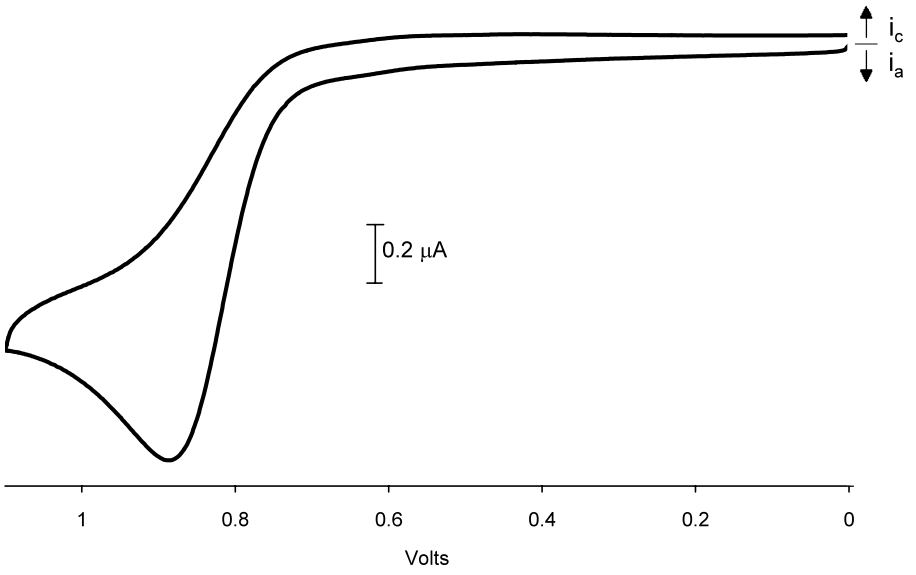

Fig. 4. Cyclic voltammogram of 0.50 mM dppr at 100 mV s^{-1} in DCM at 0.0 °C with 0.050M $[NBu_4]^+[B(C_6F_5)_4]^-$ supporting electrolyte.

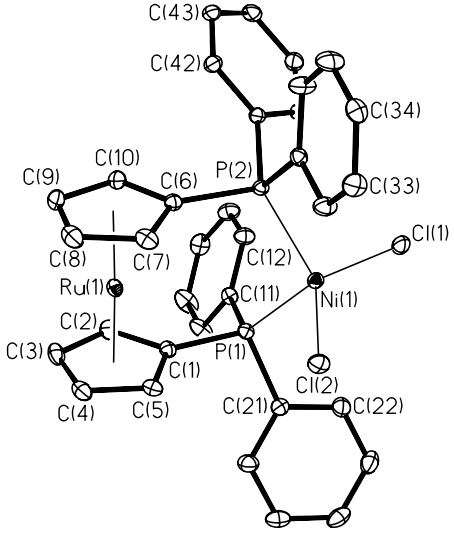

Fig. 5. An ORTEP of the molecular structure of $[NiCl_2(dppr)]$.

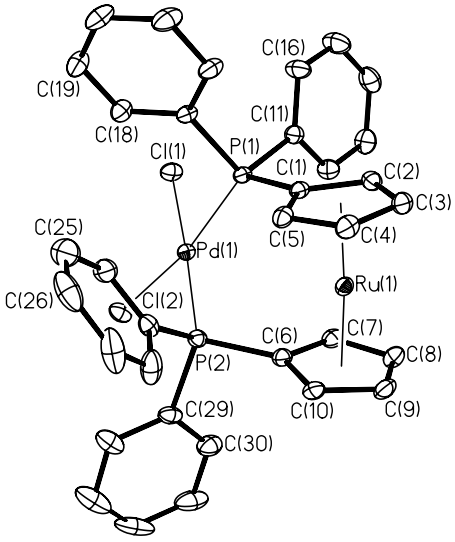

Fig. 6. An ORTEP of the molecular structure of $[PdCl_2(dppr)]$.

The structure of dppr has been determined, and the larger separation (approximately 0.3 Å) of the cyclopentadienyl rings in dppr is anticipated to give dppr a larger bite angle than dppf [11]. There are few structural reports of compounds that contain a dppr ligand. The structures of $PtRu_3(CO)_6(\mu\text{-}CO)_2(\eta^2\text{-dppf})(\mu_4\text{-}S)_2$ and $PtRu_3(CO)_6(\mu\text{-}CO)_2(\eta^2\text{-dppr})(\mu_4\text{-}S)_2$ have been determined and in both compounds the bidentate phosphine is bound to Pt [31]. The phosphine bite angle, Pt–P bond lengths and average M-centroid distance are all larger for the dppr compound. The centroid-M-centroid for dppf is 178.1° and for dppr it is 176.6°, indicating that the rings of dppr are significantly distorted from parallel. In addition, the structure of $[RuCp(dppr)CO]PF_6$ suggests that dppr has a larger bite angle than dppf in similar compounds [32]. The only other reported structure of a compound with a dppr ligand is $[PtCl_2(dppr)]$ [16].

In the report of the structure of $[PtCl_2(dppr)]$, the authors state that the palladium analogue 'would be of higher catalytic interest' [16]. Of particular interest would be the bite angle of the dppr ligand. The large bite angle of dppf in Pd(II) compounds has been proposed to facilitate fast reductive elimination to form C–C bonds [13] and sulfides [33]. However, the larger bite angle of dppr has also been proposed to promote dissociation, which decreases catalyst efficiency [34]. The bite angle of dppr in [(dppr)PdMe(CH = CAr)] was estimated to be 105–110°, which is significantly larger than the typical dppf bite angle of 97° for dppf

Table 2
Selected bond angles (°) and lengths (Å) for [MCl_2(dppM′)]

	M = Ni		M = Pd		M = Pt	
M′	Fe	Ru	Fe	Ru	Fe	Ru
Reference	[14]	this work	[15]	this work	[16]	[11]
P–M–P (°)	105.0(1)	108.005(18)	97.98(4)	100.02(17)	99.3(1)	101.0(1)
Cl–M–Cl (°)	124.5(1)	123.65(2)	89.96(4)	90.14(17)	86.3(1)	85.6(1)
X_A–M′–X_B [a] (°)	175.5 [b]	177.8	176.6	175.7	178.3	176.4 [b]
P–M′–P (°)	63.6 [b]	64.5	61.5	62.1	60.9	61.3 [b]
τ [c] (°)	9	8.4	34.1	39.3	32.3	31.8[b]
θ [d] (°)	4.5	2.1	6.2	9.2	5.9	8.8
Avg. P–M (Å)	2.223	2.3262	2.284	2.305	2.256	2.271
Avg. M–Cl (Å)	2.311	2.2209	2.349	2.358	2.404	2.348
P–P (Å)	3.668	3.764	3.43	3.531	3.438	3.504
Avg. δ_P [e] (Å)	−0.048 [b]	−0.048	0.048	0.088	−0.0052	0.025

[a] Centroid–Fe–centroid.
[b] Determined from the published structural data using ORTEP-3 for Windows [30].
[c] The torsion angle C_A–X_A–X_B–C_B where C is the carbon bonded to the P and X is the centroid.
[d] The dihedral angle between the two Cp rings.
[e] Deviation of the P atom from the Cp plane, a positive value meaning the P is closer to the Fe/Ru.

analogues [13]. The dppr bite angle determined for [$PdCl_2$(dppr)] is much smaller than the estimated range, and for the series of Group 10 metal compounds the bite angle of dppr is only 1–3° larger than that of dppf. This variation is similar to what was observed for $PtRu_3(CO)_6(\mu\text{-}CO)_2$(bidentate phosphine)$(\mu_4\text{-}S)_2$, where the bite angle of dppr is 2.1° larger than that of dppf [31]. The larger bite angle of dppr does lead to longer M–P distances and P–Ru–P angles that are larger than the corresponding P–Fe–P angles. In addition, the Cl–M–Cl angles are generally smaller for dppr, however the angles are not significantly different in [$PdCl_2$(dppf)] and [$PdCl_2$(dppr)].

The effect of the bite angle has been investigated in the amination of aryl bromides using [$PdCl_2$(bidentate phosphine)] catalysts [35]. In that system, the observation that [$PdCl_2$(dppf)] is a superior catalyst to [$PdCl_2$(dppr)] and [$PdCl_2$(DPPDPE)] (DPPDPE = $Ph_2P(o\text{-}C_6H_4\text{–}O\text{–}o\text{-}C_6H_4)PPh_2$) was attributed to the smaller bite angle of dppf (99.0°) as compared to the other two bidentate phosphines (101°). In that study, the bite angle reported for the [$PdCl_2$(dppr)] is in fact that of the Pt analogue. The actual bite angle for dppr falls precisely between dppf and DPPDPE, yet in terms of the catalytic results, dppr clearly behaves more like DPPDPE.

In addition to the bite angle, there are a number of other structural parameters commonly investigated in dppf structures. The twist angle, τ, is a measure of the relationship of the phosphorus atoms to each other and whether the Cp rings are eclipsed or staggered [1,36]. The structures of [$NiCl_2$(dppf)] and [$NiCl_2$(dppr)] are synperiplanar eclipsed, which is defined as having eclipsed Cp rings, eclipsed phosphorus atoms, and a τ angle of less than 18°. This conformation is uncommon for dppf and is previously unreported for dppr. The Pd and Pt analogues with dppf and dppr display a synclinal staggered confirmation, which is the most common conformation for chelating dppf [36]. In this arrangement, the Cp rings are staggered and the τ angle is in the range of 18–54°.

The dihedral angle between the two Cp rings, θ, is a measurement of how parallel the Cp rings are [1,36]. For compounds containing dppf, the values of θ range from 0.2 to 9.3° [1,36]. The θ values for the compounds containing dppr fit well within this range. A general trend that square planar compounds display larger values of θ than similar tetrahedral compounds has been noted for dppf [1] and is also seen here for dppr. The distance, δ, measures how far a phosphorus atom is out of the plane of the Cp ring, with a negative value indicating the phosphorus is closer to the metal of the metallocene [1]. For square planar compounds containing dppf, both phosphorus atoms typically have negative δ values while for tetrahedral compounds, one is positive and the other negative [1]. The same general pattern is observed for dppr in [MCl_2(dppr)] (M = Ni, Pd or Pt).

To further investigate the effect of coordination on dppr, the oxidative electrochemistry of the [MCl_2(dppr)] compounds was studied by cyclic voltammetry. All of the compounds displayed irreversible oxidation waves attributed to the Ru center. Since these compounds display irreversible oxidations, the $E_{1/2}$ can not be determined accurately from the E_p values [37]. Therefore, it is best to consider the trends in the oxidation potential rather then the E_p values. The E_p values for dppr typically occur at more positive potentials upon coordination of dppr to a metal center. Since dppr donates electron density to the metal to which it binds, the oxidation of the ruthenium center should be more difficult. Both the metal to which dppr bonds and the

geometry around that metal appear to influence the oxidation potential. The square planar [MCl_2(dppr)] (M = Pd or Pt) compounds in this study exhibit higher oxidation potentials than the tetrahedral [$NiCl_2$(dppr)]. The P–M–P angles are very similar for the Pd and Pt compounds, but approximately 7° smaller than the Ni compound. This difference in coordination environment may be linked to the observed differences in oxidation potential.

The electrochemistry of the [MCl_2(dppf)] analogues of these compounds is reported in 1,2-dichloroethane at 0.3 V s^{-1} using [NBu_4][ClO_4] as the supporting electrolyte [7]. The oxidation of [$NiCl_2$(dppf)] is reported to be irreversible, however the oxidation potential is not reported. For comparative purposes, we determined the oxidation potential of [$NiCl_2$(dppf)] using our conditions. The difference between the oxidation potential of the Group 10 compounds and the free phosphine can be defined as ΔE_{Fe} for dppf and ΔE_{Ru} for dppr. The reversible oxidations of [MCl_2(dppf)] (M = Pd or Pt) have a ΔE_{Fe} of 0.39 V, while the irreversible oxidation of [$NiCl_2$(dppf)] has a ΔE_{Fe} of 0.07 V. The similarity of the oxidation potentials for the Pd and Pt compounds was also seen in the dppr system. However, the ΔE_{Ru} of the dppr compounds is 0.52 V more positive than uncoordinated dppr. The ΔE_{Ru} of [$NiCl_2$(dppr)] is 0.15 V which is significantly smaller than the Pd and Pt analogues, but like the Pd and Pt species, larger than the ΔE_{Fe} of the dppf analogue.

3. Conclusions

The electrochemistry of dppf in DCM with a non-interacting supporting electrolyte displays a chemically irreversible oxidation. The chemical reaction is a dimerization and based on experimental and simulated data, the activation parameters have been determined. The oxidative electrochemistry of the Ru analogue, dppr, is irreversible. To investigate the bonding of dppr, a series of Group 10 metal compounds were prepared. The structures of [MCl_2(dppr)] (M = Ni and Pd) were determined and, along with the previously reported [$PtCl_2$(dppr)] [11], were compared to the analogous dppf compounds. The dppr and dppf compounds of Ni are tetrahedral while the Pd and Pt compounds are square planar. In this series, the bite angle of dppr is approximately 2° larger than that of dppf. In addition to the structural study, the oxidative electrochemistry of the dppr compounds was investigated and determined to be irreversible. The oxidation potentials were more positive than that of dppr, reflecting the electron withdrawing nature of the Group 10 metal. The oxidation potentials of the dppr-containing compounds are more positive than the dppf analogues and for a given metal, the ΔE_{Ru} is larger than the corresponding ΔE_{Fe}. For both dppf and dppr, the Ni compound has the smallest ΔE while the Pd and Pt compounds have identical ΔE values. It would seem that the metallocene backbone of the phosphine is more sensitive to the coordination environment as compared to the metal to which the phosphine is bound.

4. Experimental

HPLC grade DCM was purchased from Aldrich and distilled from CaH_2 under argon before use. $Li[B(C_6F_5)_4]\cdot(OEt_2)_{2.5}$ was purchased from Boulder Scientific Co. and metathesized to the tetrabutylammonium salt according to the literature procedure [21b]. NBu_4PF_6 was purchased from Aldrich and dried under vacuum prior to use. Ruthenocene and dppf were purchased from Strem Chemicals, Inc. [$NiCl_2$(dppf)] was obtained from Aldrich.

4.1. Synthesis

The preparation of dppr and [MCl_2(dppr)] (M = Ni, Pd or Pt) were carried out according to the literature procedures [16]. Additional spectroscopic characterization of [$NiCl_2$(dppr)] was carried out. The UV–Vis spectrum of [$NiCl_2$(dppr)] in DCM was obtained using a Varian Cary 300 UV–Vis spectrometer. The λ_{max} occurs at 405 nm with an extinction coefficient of 2300 cm^{-1} M^{-1}, similar to the dppf analogue (405 nm and 3000 cm^{-1} M^{-1}) [7]. Additional peaks were observed at 537 nm (420 cm^{-1} M^{-1}) and 857 nm (150 cm^{-1} M^{-1}). Furthermore, the magnetic moment of this paramagnetic compound was determined using the Evans method on a JEOL Eclipse 400 FT-NMR [25,26].

4.2. X-ray crystallography

Crystals of [$NiCl_2$(dppr)] were obtained by slow vapor diffusion of ether into a DCM solution of the compound. Crystals of [$PdCl_2$(dppr)]·CH_2Cl_2 were obtained by dissolving in DCM, layering with ether, placing the flask in a dewar filled with acetone, and slowly cooling in a freezer. Crystallographic data are collected in Table 3. Green plates of [$NiCl_2$(dppr)] belonged to the triclinic crystal system and the centrosymmetric alternative was initially chosen and later verified by the results of refinement. Yellow blocks of [$PdCl_2$(dppr)]·CH_2Cl_2 belonged to the monoclinic system and the space group was uniquely assigned from systematic absences. Data were collected with a Bruker platform system with an APEX detector and monocap collimator. Empirical corrections for absorption were provided by the program SADABS. Both structures were solved by direct methods and refined with anisotropic thermal parameters for all non-hydrogen atoms. All software is

Table 3
Crystal data and structure analysis results

	$[NiCl_2(dppr)]$	$[PdCl_2(dppr)]\cdot CH_2Cl_2$
Formula	$C_{34}H_{28}Cl_2NiP_2Ru$	$C_{35}H_{30}Cl_4P_2PdRu$
Formula weight	729.18	861.80
Temperature (K)	218(2)	223(2)
Crystal system	triclinic	monoclinic
Space group	$P\bar{1}$	$P2_1/c$
a (Å)	9.6420(4)	9.880(3)
b (Å)	9.6737(4)	18.476(5)
c (Å)	18.2027(7)	19.171(6)
α (°)	101.166(1)	90
β (°)	95.369(1)	103.34(6)
γ (°)	114.720(1)	90
V (Å^3)	1483.75(10)	3406.2(17)
Z	2	4
Crystal size (mm)	$0.25 \times 0.25 \times 0.10$	$0.15 \times 0.15 \times 0.05$
Crystal color	green	yellow
Radiation; λ (Å)	0.71073	0.71073
θ Range (°)	2.33–28.29	2.12–27.99
Data collected	$-12 \le h \le 12$, $-12 \le k \le 12$, $-23 \le l \le 24$	$-12 \le h \le 13$, $-21 \le k \le 23$, $-18 \le l \le 25$
No. of data collected	11 257	17 335
No. of unique data	6947	7328
Absorption correction	SADABS	SADABS
Final R indices (obs. data)	$R_1 = 0.0278$, $wR_2 = 0.0814$	$R_1 = 0.0346$, $wR_2 = 0.0871$
Goodness of fit	1.160	1.091

contained in libraries distributed by Bruker AXS (Madison, WI).

4.3. Electrochemistry

The electrochemistry was conducted using a Princeton Applied Research 263-A potentiostat. A blanket of argon was kept over the solutions for the duration of the experiments. The 1.5-mm glassy carbon working electrode was polished with 1 μm diamond paste, rinsed with acetone, and then polished with 1/4 μm diamond paste. Prior to use, the working electrode was washed with DCM. A platinum wire served as the counter electrode and a non-aqueous silver/silver chloride electrode as the reference electrode. The electrochemical potentials were collected and analyzed using power suite.

The oxidative electrochemistry of dppf was investigated in DCM. Analyte concentrations of 0.50, 1.0, 5.0 and 10.0 mM in 10.0 ml of DCM each contained 0.050 M $[NBu_4]^+[B(C_6F_5)_4]^-$ as the supporting electrolyte. Scans were made at 10, 25, 50, and 75 mV s^{-1} and then from 100 to 1000 mV s^{-1} at intervals of 100 mV s^{-1}. For each concentration, this series of scans was made at -10, 0, 10, and 20 °C. A jacketed cell connected to a temperature controlled circulating bath was used to maintain the temperature of the solution within 0.1 °C. Decamethylferrocene was added as internal standard near the end of the experiment [38]. The analyte potential was referenced to ferrocene by subtracting 0.62 V [21c]. This value can then be referenced to the NHE by adding 0.66 V [17]. The chemically reversible oxidation of dppf occurs at 0.23 V vs. $Fc^{0/+}$.

The oxidative electrochemistry of dppr was studied in 10.0 ml of DCM at two concentrations (0.50 mM, and 4.0 mM) and temperatures (0.0 and 25.0 °C) using 0.050 M $[NBu_4]^+[B(C_6F_5)_4]^-$ as the supporting electrolyte. The oxidation of dppr is irreversible and has an anodic peak potential of 0.44 V vs. $Fc^{0/+}$ at 0.1 V s^{-1} and 25.0 °C. The oxidative electrochemistry of the Group 10 metal complexes, $[MCl_2(dppr)]$ (M = Ni, Pd or Pt) and $[NiCl_2(dppf)]$, was examined in DCM. The analyte concentration was 1.0 mM in 10.0 ml of DCM and the supporting electrolyte was 0.1 M $[NBu_4]^+[PF_6]^-$. Both $[NiCl_2(dppf)]$ and the dppr compounds showed irreversible oxidation waves. At 0.1 V s^{-1} and 25.0 °C the E_p vs. $Fc^{0/+}$ for $[NiCl_2(dppr)]$ occurs at 0.59 V, the Pd and Pt analogues were observed at 0.96 V and the wave for $[NiCl_2(dppf)]$ is at 0.30 V.

5. Supplementary material

Crystallographic data (CIF files) for the structural analysis have been deposited with the Cambridge Crystallographic Data Centre, CCDC no. 200 352 for $[NiCl_2(dppr)]$ and CCDC no. 200 353 for $[PdCl_2(dppr)]\cdot CH_2Cl_2$. Copies of this information may be obtained free of charge from The Director, CCDC, 12 Union Road, Cambridge CB2 1EZ, UK (Fax: +44-1223-336033; e-mail: deposit@ccdc.cam.ac.uk or www: http://www.ccdc.cam.ac.uk).

Acknowledgements

C.N., A.N.C. and M.A.F. would like to thank Dr W.E. Geiger (University of Vermont) for his assistance with the simulations, the Applied Research Committee (Lafayette College) for its support through an EXCEL scholarship, the donors of the Petroleum Research Fund, administered by the American Chemical Society, for partial support of this research and the Kresge Foundation for the purchase of the Jeol Eclipse 400 MHz NMR.

References

[1] K.-S. Gan, T.S.A. Hor, in: A. Togni, T. Hayashi (Eds.), Ferrocenes (Chapter 1), VCH, New York, 1995.
[2] R.T. Hembre, J.S. McQueen, V.W. Day, J. Am. Chem. Soc. 118 (1996) 798.

[3] D.L. DuBois, C.W. Eigenbrot, Jr., A. Miedaner, J.C. Smart, R.C. Haltiwanger, Organometallics 5 (1986) 1405.
[4] C.E. Housecroft, S.M. Owen, P.R. Raithby, B.A.M. Shaykh, Organometallics 9 (1990) 1617.
[5] A. Greff, P. Diter, D. Guillaneux, H.B. Kagan, New. J. Chem. 21 (1997) 1353.
[6] (a) T.M. Miller, K.J. Ahmed, M.S. Wrighton, Inorg. Chem. 28 (1989) 2347;
(b) P. Zanello, G. Opromolla, G. Giorgi, G. Sasso, A. Togni, J. Organomet. Chem. 506 (1996) 61;
(c) D.S. Shephard, B.F.G. Johnson, A. Harrison, S. Parsons, S.P. Smidt, L.J. Yellowlees, D. Reed, J. Organomet. Chem. 563 (1998) 113.
[7] B. Corain, B. Longato, G. Favero, D. Ajò, G. Pilloni, U. Russo, F.R. Kreissl, Inorg. Chim. Acta 157 (1989) 259.
[8] G. Pilloni, B. Longato, B. Corain, J. Organomet. Chem. 420 (1991) 57.
[9] A.E. Gerbase, E.J.S. Vichi, E. Stein, L. Amaral, A. Vasquez, M. Hörner, C. Maichle-Mössmer, Inorg. Chim. Acta 266 (1997) 19.
[10] M.G. Hill, W.M. Lamanna, K.R. Mann, Inorg. Chem. 30 (1991) 4687.
[11] S. Li, B. Wei, P.M.N. Low, H.K. Lee, T.S.A. Hor, F. Xue, T.C.W. Mak, J. Chem. Soc. Dalton Trans. (1997) 1289.
[12] B.C. Hamann, J.F. Hartwig, J. Am. Chem. Soc. 120 (1998) 3694.
[13] J.M. Brown, P.J. Guiry, Inorg. Chim. Acta 220 (1994) 249.
[14] U. Casellato, D. Ajó, G. Valle, B. Corain, B. Longato, R. Graziani, J. Cryst. Spect. Res. 18 (1988) 583.
[15] T. Hayashi, M. Konishi, Y. Kobori, M. Kumada, T. Higuchi, K. Hirotsu, J. Am. Chem. Soc. 106 (1984) 158.
[16] D.A. Clemente, G. Pilloni, B. Corain, B. Longato, M. Tiripicchio-Camellini, Inorg. Chim. Acta 115 (1986) L9.
[17] S. Lu, V.V. Strelets, M.F. Ryan, W.J. Pietro, A.B.P. Lever, Inorg. Chem. 35 (1996) 1013.
[18] C. Hansch, A. Leo, R.W. Taft, Chem. Rev. 91 (1991) 165.
[19] M.L. Olmstead, R.G. Hamilton, R.S. Nicholson, Anal. Chem. 41 (1969) 260.
[20] D.R. Lide, Handbook of Organic Solvents (Chapter 13), CRC Press, Boca Raton, 1994.
[21] (a) N. Camire, A. Nafady, W.E. Geiger, J. Am. Chem. Soc. 124 (2002) 7260;
(b) R. LeSuer, W.E. Geiger, Angew. Chem. Int. Ed. Engl. 39 (2000) 248;
(c) N. Camire, U.T. Mueller-Westerhoff, W.E. Geiger, J. Organomet. Chem. 637–639 (2001) 823.
[22] A. Lasia, J. Electroanal. Chem. 146 (1983) 413.
[23] B.M. Ramachandran, S.M. Trupia, W.E. Geiger, P.J. Carroll, L.G. Sneddon, Organometallics 21 (2002) 5078.
[24] (a) U. Koelle, A. Salzer, J. Organomet. Chem. 243 (1983) C27;
(b) U. Koelle, J. Grub, J. Organomet. Chem. 289 (1985) 133;
(c) A. Pederson, V. Skagestad, M. Tilset, Acta Chem. Scand. 49 (1995) 632;
(d) M.F. Ryan, D.E. Richardson, D.L. Lichtenberger, N.E. Gruhn, Organometallics 13 (1994) 1190;
(e) D. Wang, R.J. Angelici, J. Am. Chem. Soc. 118 (1996) 935.
[25] G.S. Girolami, T.B. Rauchfuss, R.J. Angelici, In Synthesis and Technique in Inorganic Chemistry, third ed., University Science Books, Sausalito, 1999, p. 117.
[26] The $CHCl_3$ peak separation was 38.4 Hz for a 0.40 mM.
[27] G.L. Miessler, D.A. Tarr, In Inorganic Chemistry, second ed., Prentice Hall, Upper Saddle River, 1999, p. 315.
[28] Y.S. Sohn, D.N. Hendrickson, H.B. Gray, J. Am. Chem. Soc. 74 (1971) 3603.
[29] S. Akabori, T. Kumagai, T. Shirahige, S. Sato, K. Kawazoe, C. Tamura, M. Sato, Organometallics 6 (1987) 526.
[30] L.J. Farrugia, J. Appl. Cryst. 30 (1997) 565.
[31] S.-W.A. Fong, J.J. Vittal, T.S.A. Hor, Organometallics 19 (2000) 918.
[32] S.P. Yeo, W. Henderson, T.C.W. Mak, T.S.A. Hor, J. Organomet. Chem. 575 (1999) 171.
[33] G. Mann, D. Baranano, J.F. Hartwig, A.L. Rheingold, I.A. Guzei, J. Am. Chem. Soc. 120 (1998) 9205.
[34] B. Wei, T.S.A. Hor, J. Mol. Catal. A: Chem. 132 (1998) 223.
[35] B.C. Hamann, J.F. Hartwig, J. Am. Chem. Soc. 120 (1998) 3694.
[36] G. Bandoli, A. Dolmella, Coord. Chem. Rev. 109 (2000) 161.
[37] A.J. Bard, L.R. Faulkner, Electrochemical Methods, Fundamentals and Applications, second ed. (Chapter 6), Wiley, New York, 2001.
[38] The ferrocene potential was too close to that of dppf, so decamethylferrocene was used as the internal standard.